Available online at www.sciencedirect.com
ScienceDirect
Journal of Computational Physics 227 (2007) 156–173
JOURNAL OF COMPUTATIONAL PHYSICS
www.elsevier.com/locate/jcp

A computational error-assessment of central finite-volume discretizations in large-eddy simulation using a Smagorinsky model

J. Meyers [a,b,*], B.J. Geurts [c,d], P. Sagaut [a]

[a] D'Alembert Institute, Université Pierre et Marie Curie – Paris 6, Boîte 162, 4 Place Jussieu, 75252 Paris cedex 05, France
[b] Department of Mechanical Engineering, Katholieke Universiteit Leuven, Celestijnenlaan 300A – Bus 2421, B3001 Leuven, Belgium
[c] Multiscale Modeling and Simulation, Faculty EEMCS, University of Twente, P.O. Box 217, 7500 AE Enschede, The Netherlands
[d] Anisotropic Turbulence, Department of Applied Physics, Eindhoven University of Technology, P.O. Box 513, NL-5600 MB Eindhoven, The Netherlands

Received 10 November 2006; received in revised form 4 July 2007; accepted 21 July 2007
Available online 1 August 2007

Abstract

We present a framework for the computational assessment and comparison of large-eddy simulation methods. We apply this to large-eddy simulation of homogeneous isotropic decaying turbulence using a Smagorinsky subgrid model and investigate the combined effect of discretization and model errors at coarse subgrid resolutions. We compare four different central finite-volume methods. These discretization methods arise from the four possible combinations that can be made with a second-order and a fourth-order central scheme for either the convective and the viscous fluxes. By systematically varying the simulation resolution and the Smagorinsky coefficient, we determine parameter regions for which a desired number of flow properties is simultaneously predicted with approximately minimal error. We include both physics-based and mathematics-based error definitions, leading to different error-measures designed to emphasize either errors in large- or in small-scale flow properties. It is shown that the evaluation of simulations based on a single physics-based error may lead to inaccurate perceptions on quality. We demonstrate however that evaluations based on a range of errors yields robust conclusions on accuracy, both for physics-based and mathematics-based errors. Parameter regions where all considered errors are simultaneously near-optimal are referred to as 'multi-objective optimal' parameter regions. The effects of discretization errors are particularly important at marginal spatial resolution. Such resolutions reflect local simulation conditions that may also be found in parts of more complex flow simulations. Under these circumstances, the asymptotic error-behavior as expressed by the order of the spatial discretization is no longer characteristic for the total dynamic consequences of discretization errors. We find that the level of overall simulation errors for a second-order central discretization of both the convective and viscous fluxes (the '2–2' method), and the fully fourth-order ('4–4') method, is equivalent in their respective 'multi-objective optimal' regions. Mixed order methods, i.e. the '2–4' and '4–2' combinations, yield errors which are considerably higher.

Keywords: Large-eddy simulation; Smagorinsky model; Turbulence; Discretization errors; Error-landscape

* Corresponding author. Address: Department of Mechanical Engineering, Katholieke Universiteit Leuven, Celestijnenlaan 300A – Bus 2421, B3001 Leuven, Belgium.
E-mail addresses: johan.meyers@mech.kuleuven.be (J. Meyers), b.j.geurts@utwente.nl (B.J. Geurts), sagaut@lmm.jussieu.fr (P. Sagaut).

0021-9991/$ - see front matter
doi:10.1016/j.jcp.2007.07.012

1. Introduction

In recent years, large-eddy simulation (LES) has become established as a research tool for turbulent flows [1,2]. Currently, an increasing number of LES studies is oriented towards industrial applications, often based on a finite-volume discretization. However, several fundamental issues remain to be solved in LES in order to develop strict reliability and quality verifications. The use of finite-volume discretization methods is complicated by the absence of a proper estimation of errors in LES. Specifically at coarse simulation resolutions, mostly dictated by available computer resources, this poses an obstacle for assuring objective quality guidelines for LES. We focus on this issue here.

In the present paper, we will use a new analysis tool for the evaluation of LES error-behavior. This is a computational method of error-analysis, aimed at quantifying the incurred error in a particular large-eddy simulation. Such measuring of errors in a simulation is a pre-cursor for the optimization of errors. Four different numerical discretization schemes are evaluated and compared for LES using the Smagorinsky model. Simulation errors are defined either based on strict mathematical principles, or on physics-based simulation properties. The latter are usually the only ones which are accessible in practical applications. However, we find that the perceived LES quality strongly depends on the particular error definition that is used. Specifically, evaluations of LES using physics-based errors may lead to an overly optimistic assessment, due to partially compensating sources of error. Despite this, we find that the simultaneous inclusion of a *range* of physics-based errors, emphasizing both large- and small-scale flow properties, does allow a robust qualification of the different discretization schemes which is quite independent of the error definition. In this way, a complete assessment of the total simulation error in LES associated with a particular finite-volume discretization can be achieved.

The new evaluation method, which is here illustrated with simulations of homogeneous isotropic turbulence, leads to further insights into error behavior of Smagorinsky LES. In particular, the computational error-assessment allows to analyze the error-behavior at coarse resolutions. This regime is unattainable to existing methods of analysis and can display surprising effects of interacting errors. First of all, we consider the combination of a fourth-order discretization of the convective terms with a second-order discretization of the viscous terms in the LES equations. This is often used in higher-order extensions of CFD codes. We find, rather unexpectedly that this leads to worse LES results. Secondly, improving the order of the discretization scheme in LES does not necessarily mean improving the quality of the solution. In terms of the optimal achievable error-level of a method, quite equivalent error-levels are observed for second- and fourth-order discretizations. These results are most pronounced at coarse resolutions and will be further elucidated in the current manuscript.

In order to arrive at computationally affordable calculations, LES aims to predict accurate turbulent flow statistics by simulating flows at spatial and temporal resolutions which are much coarser than those needed for the direct numerical simulation of the Navier–Stokes equations [3]. Mathematically, this is formalized by filtering the Navier–Stokes equations with a low-pass filter. Consequently, the filtered equations can be numerically approximated on a much coarser grid, with a mesh spacing h which can be chosen on the order of the selected filter width Δ. The filtering operation leads to a set of unclosed stress terms in the equations (i.e., the subgrid-scale stresses) which are modelled with a subgrid-scale model [1,2].

Much of the subgrid modelling in LES is motivated by the proposition that small-scale turbulence in high-Reynolds number flows displays universal properties [4]. Consequently, it is considered possible to represent the dynamic effect of these small turbulent scales by means of a relatively simple subgrid-sale model [5]. Subgrid-scale modelling has been an important research topic in LES research during the past decennia [1].

The large-eddy approach to turbulent flows requires the discretization of the modelled equations. For complex flow problems it is popular to resort to high-order finite-volume methods. At marginal subgrid-resolution, defined here as Δ/h, such numerical treatment seriously complicates the problem. Under these resolution conditions errors introduced by the numerical discretization are of the same order of magnitude as the subgrid-scale stresses [6]. Moreover, modelling errors and discretization errors, which are non-linear terms, may interact in intricate ways, since they are coupled in an implicit way via the resolved field [7–11]. Due to their non-linear nature, these couplings escape available mathematical tools usually used to investigate numerical-scheme accuracy, leading to the need for the definition of an adequate framework.

Two discretization related error sources are identified in the literature, i.e., errors due to the finite-difference/finite-volume approximation of derivatives and aliasing errors, which arise when the non-linear terms in the Navier–Stokes equations are projected onto the solution space [6,12]. The dynamic influence of aliasing errors was, however, found to be of minor relative importance, and only relevant for very high-order discretization methods [13,14]. Consequently, most numerical error analyses in LES concentrate on errors introduced by discretization of the derivatives.

In recent years, several studies were devoted to isolating the effects of discretization errors from those of errors in the subgrid-scale modelling. As shown, e.g. in Ref. [15], discretization of the derivatives in the Navier–Stokes equations has the same effect as applying a particular implicit filter to the equations, with filter width expressed in terms of the grid spacing h. Several studies suggest that the partial inversion of this implicit filter improves the overall LES results [16,17], or at least provides a clear framework to motivate subgrid-scale closures [18]. However, in practice, such an inversion primarily operates on the leading order terms of the discretization, yielding a tensor-diffusivity reconstruction or an approximate deconvolution [19–21]. So, a focus on the total low-pass filter and its inversion can only partially clarify LES errors.

In an alternative approach, the subgrid model effects related to the filter width Δ were explicitly separated from the numerical errors associated with the grid spacing h. To this end, different proposals were made. In one class of methods $\Delta > h$ is selected and all scales between Δ and h are removed from the solution by explicit filtering [6,12]. In another class of methods, Δ is considered a parameter which is governed by the subgrid-scale model. Hence, $\Delta/h > 1$ is obtained by grid refinement, while keeping Δ in the model constant [7–9,22–24]. No further explicit filter is used to accommodate $\Delta > h$. In such an approach, it is possible to define a grid-independent LES. Discretization and modelling errors can be measured using this grid-independent LES and a DNS reference. For the Smagorinsky model, it was observed that $\Delta/h \gg 1$ does not improve the overall LES solution but, instead, leads to solutions whose accuracy is limited by deficiencies in the subgrid model [7–9]. In this framework, discretization errors and modelling errors were shown to partially cancel for $\Delta = h$ [7,9].

A more pragmatic view on modelling and discretization errors concentrates on the overall simulation errors at $\Delta = h$ [9,25,26]. By systematically varying the Smagorinsky parameter C_s, the spatial resolution N and the Reynolds number in LES of decaying homogeneous isotropic turbulence a better understanding could be obtained of the consequences of the combined errors in the subgrid modelling and discretization [9]. From this computational error-assessment the so-called error-landscape could be inferred which, in particular, allows to identify 'optimal refinement strategies' $\widehat{C}_s(N)$. These provide the optimal model parameter, resulting in the lowest simulation error in a specific flow property at given resolution. Later [25], these optimal refinement strategies were compared with the grid-dependence of the model coefficient that results from the dynamic eddy-viscosity model [27]. This showed that the dynamic coefficient over-predicts the optimal refinement strategy. From a methodological perspective, this study illustrated that the error-landscape approach is also instructional in the interpretation of the quality of other eddy-viscosity subgrid models. Recently [28] an efficient method was proposed to directly determine the optimal refinement strategy. The methodology was further extended by evaluating a set of error-measures simultaneously [26], leading to the identification of 'multi-objective optimal' refinement regions. In such parameter regions multiple simulation properties, including both large- and small-scale quantities, are predicted simultaneously nearly optimal.

In the present study, the error-landscape framework is used for the analysis of different numerical discretization schemes, used to simulate homogeneous decaying turbulence, adopting the Smagorinksy model. We will concentrate on central finite-volume schemes, discretizing the convective and viscous fluxes either with a second-order or a fourth-order discretization method. This allows four combinations, e.g. a second-order discretization of the convective fluxes, combined with a second-order discretization of the viscous fluxes. We will refer to this as the 2–2 scheme. Likewise, one may define a 4–2, 2–4 and 4–4 scheme.

In order to reduce the total simulation errors, several studies have concentrated on high-order schemes for the *convective* terms in LES, e.g. preserving total kinetic energy [29–31]. However, our results indicate that for Smagorinsky LES, mixed-order discretizations for the convective and viscous fluxes are inferior to equal-order discretizations. To our knowledge, balancing errors arising from convective and viscous discretizations in LES have never been reported. This balancing expresses the dynamic interaction between modelling and numerical errors [14]. We further show that 2–2 and 4–4 simulations provide equivalent error-levels at coarse resolutions.

This contrasts asymptotic convergence properties that apply only at sufficiently high resolutions. Likewise, 'static' error evaluations of numerical-schemes are incapable of gauging these effects and hence are less suitable for the selection of LES discretizations [14].

The organization of this paper is as follows. In Section 2, the governing equations and simulation setup are summarized. In the following Section 3, the framework for the assessment of LES errors is presented. Subsequently, in Section 4, large-eddy simulations with four different numerical-schemes, i.e., 2–2, 4–4, 4–2 and 2–4, are compared based on the error-landscape framework. A detailed interpretation of the error consequences is made in terms of the predicted spectra of kinetic energy. Finally, in Section 5, conclusions are presented.

2. Governing equations and setup

The spatially filtered Navier–Stokes equations for incompressible flows can be written in dimensionless form as

$$\begin{aligned} &\frac{\partial \bar{u}_i}{\partial x_i} = 0, \\ &\frac{\partial \bar{u}_i}{\partial t} + \frac{\partial \bar{u}_i \bar{u}_j}{\partial x_j} + \frac{\partial \bar{p}}{\partial x_i} - \frac{2}{Re}\frac{\partial \overline{S}_{ij}}{\partial x_j} - \frac{\partial \tau_{ij}}{\partial x_j} = 0; \quad i = 1,2,3 \end{aligned} \tag{1}$$

where $\bar{u}_i$ is the filtered velocity component in the x_i-direction, $\bar{p}$ the filtered pressure and Re the Reynolds number. The LES filter is assumed to have a width Δ and is denoted by $\overline{(\cdot)}$. Moreover, $\overline{S}_{ij} = [\partial \bar{u}_i/\partial x_j + \partial \bar{u}_j/\partial x_i]/2$ corresponds to the filtered strain-rate tensor.

The filtering of the Navier–Stokes equations gives rise to the subgrid-scale stress tensor τ_{ij}. This is an unclosed term in the equations, that depends on both the filtered and the unfiltered velocity field. It is given by

$$\tau_{ij} = \bar{u}_i \bar{u}_j - \overline{u_i u_j}. \tag{2}$$

In large-eddy simulations, these subgrid-scale stresses are replaced by a model m_{ij}, which approximates the dynamic effect of the subgrid-scales on the resolved scales. Such a closure model is based on operations acting on the resolved velocity field $\bar{u}_i$ alone.

One of the earliest and most often employed formulations for m_{ij} is the Smagorinsky model [32], which approximates the deviatoric part of τ_{ij} as

$$m_{ij} = 2(C_s \Delta)^2 |\overline{S}| \overline{S}_{ij}, \tag{3}$$

with C_s the Smagorinsky coefficient, Δ the LES filter width and $|\overline{S}| = (2\overline{S}_{ij}\overline{S}_{ij})^{1/2}$ the magnitude of the filtered strain-rate tensor.

To investigate the dynamical effects of errors in the subgrid modelling and the numerical discretization we carry out computations of decaying homogeneous isotropic turbulence at a number of resolutions and different values for the model parameter C_s. We closely follow the 'error-landscape' procedure proposed in [9]. In this paper, we focus on effects due to the spatial discretization and consider a number of different numerical discretization methods. The Reynolds number in the current study corresponds to an initial $Re_\lambda = 100$ in terms of the Taylor–Reynolds number Re_λ. The initial turbulent kinetic energy is 0.5. In the DNS reference, the energy decays from its initial level to 0.15, corresponding approximately to two eddy turnover times. During this time, the Taylor–Reynolds number decreases to 54. Full details of the DNS reference, including a comprehensive grid-convergence analysis of the results may be found in Ref. [9].

The initial fields for the large-eddy simulations are obtained by filtering the initial DNS field [9] with a cubical sharp cut-off filter. The filter cut-off is related to the grid cut-off wavenumber $k_c = \pi/h$, with h the grid spacing. During the simulations, no additional explicit filtering is performed and for the implementation of the Smagorinsky model, we further take $\Delta = h$. All computations are performed in a non-dimensional computational box with size one. Hence, the grid spacing h corresponds with $1/N$, with N^3 the total number of mesh points in the computational domain.

The large-eddy simulation and the reference direct numerical simulation [9] are performed with a compressible Navier–Stokes solver, at a low Mach number $M = 0.2$. At this Mach number, compressibility effects are

negligible. Hence, the model (3) does not need to be supplemented with a model for the trace of τ_{ij} and the subgrid-scale terms in the energy equation are negligible [33].

We adopt cell-centered finite-volume discretizations combined with a four-stage, second-order accurate Runge–Kutta time integration [2]. We next present a brief overview of the different spatial discretization schemes. These have been extensively applied to compressible turbulence in Refs. [7,34,35,9]. We distinguish between second- and fourth-order accurate methods for the convective and the viscous fluxes. In total, this yields four possible combinations. The second-order schemes correspond to an often used finite-volume implementation of the equations using a cell-centered discretization and a trapezoidal rule for the integration of the fluxes [36,37]. Equivalently, these schemes may be formulated using weighted central differences [7,15] and we will follow this approach here. The fourth-order schemes which are considered, are logical high-order extensions of the second-order schemes, such that a consistent family of second- and fourth-order discretizations for the convective and viscous terms is obtained for analysis in the current study. We turn to the treatment of the convective terms first and describe the discretization of the viscous fluxes afterwards.

For the discretization of the convective fluxes the adopted second-order discretization corresponds to

$$\left.\frac{\partial f}{\partial x}\right|_{i,j,k} = \frac{r_{i+1,j,k} - r_{i-1,j,k}}{2h}, \tag{4}$$

$$\text{where } r_{i,j,k} = \frac{1}{2}s_{i,j,k} + \frac{1}{2}\frac{s_{i,j+1,k} + s_{i,j-1,k}}{2}, \tag{5}$$

$$\text{with } s_{i,j,k} = \frac{1}{2}f_{i,j,k} + \frac{1}{2}\frac{f_{i,j,k+1} + f_{i,j,k-1}}{2}, \tag{6}$$

where $f_{i,j,k}$ is the convective flux-vector at node (i,j,k). Here, it is understood that the coordinate direction x corresponds to index i and similarly y, z correspond to j and k. One may recognize a second-order accurate central finite-difference scheme in (4). This scheme is applied to the intermediate field $r_{i,j,k}$ that is obtained by interpolation of the flux-vector field $f_{i,j,k}$ in directions perpendicular to the direction with respect to which the derivative is evaluated. This additional averaging over j and k increases the robustness of the scheme and removes the occurrence of π-modes which may arise from the use of 1D schemes in each direction of space [7,34,38]. It is worth noting that such fully multidimensional schemes are similar to those deduced from multidimensional finite-element analysis. The derivatives with respect to y and z may be defined analogously and will not be specified explicitly here.

The fourth-order convective discretization corresponds to

$$\left.\frac{\partial f}{\partial x}\right|_{i,j,k} = \frac{4}{3}\frac{r_{i+1,j,k} - r_{i-1,j,k}}{2h} - \frac{1}{3}\frac{r_{i+2,j,k} - r_{i-2,j,k}}{4h}, \tag{7}$$

$$\text{where } r_{i,j,k} = \frac{5}{8}s_{i,j,k} + \frac{1}{2}\frac{s_{i,j+1,k} + s_{i,j-1,k}}{2} - \frac{1}{8}\frac{s_{i,j+2,k} + s_{i,j-2,k}}{2}, \tag{8}$$

$$\text{with } s_{i,j,k} = \frac{5}{8}f_{i,j,k} + \frac{1}{2}\frac{f_{i,j,k+1} + f_{i,j,k-1}}{2} - \frac{1}{8}\frac{f_{i,j,k+2} + f_{i,j,k-2}}{2}. \tag{9}$$

This defines the fourth-order accurate central finite-difference scheme, albeit with additional fourth-order accurate interpolation applied in directions perpendicular to the direction with respect to which the derivative is evaluated. As for the second-order scheme, this increases robustness, while the formal fourth-order of the scheme is preserved [7,34].

For the discretization of the viscous terms and the subgrid-scale model, we use discretization schemes that are based on two consecutive applications of first derivatives. In fact, the first step is a derivative, which, when applied on a collocated field $f_{i,j,k}$, provides derivative results at the staggered locations $(i+\frac{1}{2}, j+\frac{1}{2}, k+\frac{1}{2})$. Second derivatives are then obtained by another use of such a first derivative but now operating on information available at locations $(i+\frac{1}{2}, j+\frac{1}{2}, k+\frac{1}{2})$ and returning the approximate derivatives at the nodes (i,j,k). Alternatively, one may view this as the application of an 'inner' and an 'outer' first derivative. For the second-order discretization, the formulation of the 'inner' derivative is [7,34]

$$\left.\frac{\partial f}{\partial x}\right|_{i+\frac{1}{2},j+\frac{1}{2},k+\frac{1}{2}} = \frac{r_{i+1,j+\frac{1}{2},k+\frac{1}{2}} - r_{i,j+\frac{1}{2},k+\frac{1}{2}}}{h}, \tag{10}$$

$$\text{where } r_{i,j+\frac{1}{2},k+\frac{1}{2}} = \frac{s_{i,j+1,k+\frac{1}{2}} + s_{i,j,k+\frac{1}{2}}}{2}, \tag{11}$$

$$\text{with } s_{i,j,k+\frac{1}{2}} = \frac{f_{i,j,k+1} + f_{i,j,k}}{2}. \tag{12}$$

This corresponds to a second-order accurate central scheme, combined with two second-order accurate interpolations in directions perpendicular to the derivative. Shifting this discrete operator over half a grid spacing yields the 'outer' derivative. In detail:

$$\left.\frac{\partial f}{\partial x}\right|_{i,j,k} = \frac{r_{i+\frac{1}{2},j,k} - r_{i-\frac{1}{2},j,k}}{h}, \tag{13}$$

$$\text{where } r_{i+\frac{1}{2},j,k} = \frac{s_{i+\frac{1}{2},j+\frac{1}{2},k} + s_{i+\frac{1}{2},j-\frac{1}{2},k}}{2}, \tag{14}$$

$$\text{with } s_{i+\frac{1}{2},j+\frac{1}{2},k} = \frac{f_{i+\frac{1}{2},j+\frac{1}{2},k+\frac{1}{2}} + f_{i+\frac{1}{2},j+\frac{1}{2},k-\frac{1}{2}}}{2}. \tag{15}$$

The sequential application of these 'inner' and 'outer' schemes yield the total, second-order accurate viscous flux treatment. Since all boundary conditions are periodic, no specific problems at the boundaries arise.

For the fourth-order accurate discretization of the viscous and subgrid-fluxes a combination of two fourth-order accurate first derivatives is used. Given collocated field data, the following scheme is used [35,9] to approximate the first derivative in the staggered locations:

$$\left.\frac{\partial f}{\partial x}\right|_{i+\frac{1}{2},j+\frac{1}{2},k+\frac{1}{2}} = \frac{27}{24}\frac{r_{i+1,j+\frac{1}{2},k+\frac{1}{2}} - r_{i,j+\frac{1}{2},k+\frac{1}{2}}}{h} - \frac{1}{8}\frac{r_{i+2,j+\frac{1}{2},k+\frac{1}{2}} - r_{i-1,j+\frac{1}{2},k+\frac{1}{2}}}{3h}, \tag{16}$$

$$\text{where } r_{i,j+\frac{1}{2},k+\frac{1}{2}} = \frac{9}{8}\frac{s_{i,j+1,k+\frac{1}{2}} + s_{i,j,k+\frac{1}{2}}}{2} - \frac{1}{8}\frac{s_{i,j+2,k+\frac{1}{2}} + s_{i,j-1,k+\frac{1}{2}}}{2}, \tag{17}$$

$$\text{with } s_{i,j,k+\frac{1}{2}} = \frac{9}{8}\frac{f_{i,j,k+1} + f_{i,j,k}}{2} - \frac{1}{8}\frac{f_{i,j,k+2} + f_{i,j,k-1}}{2}. \tag{18}$$

This corresponds to a fourth-order central scheme (16), combined with fourth-order interpolations in perpendicular directions (17) and (18). Completion of the second derivatives follows from application of the corresponding scheme, but now operating on staggered field data and returning an approximate derivative at the collocated grid locations. The specification of that scheme follows analogously to the description given above for the second-order treatment.

Based on these discretization schemes, we may now define four different discrete representations of the LES equations. In fact, these methods correspond to all possible combinations of the discretizations of the convective and viscous terms introduced in Eqs. (4)–(18). As mentioned above in the introduction, we will use the acronyms 2–2, 2–4, 4–2, 4–4, for the different combinations. The 2–2 and 4–4 schemes correspond, respectively, to a fully second-order and a fully fourth-order discretization. The 4–2 combination has been used in past LES studies of the temporal mixing layer [34,7]. Finally, the 2–4 combination is a somewhat exotic discretization, which is added for sake of completeness. Throughout, the treatment of the fluxes due to the subgrid-scales is taken identical to that of the viscous fluxes.

3. Near-optimal and multi-objective optimal regions

In this section, we introduce 'near-optimal' and 'multi-objective' parameter regions, which provide the basic context within which the overall error-behavior of an LES method will be assessed. First in Section 3.1, the basic elements are presented. Comparison of a collection of large-eddy simulations at different resolutions N and Smagorinsky constants C_s, with reference DNS data allow to construct an 'error-landscape' [9]. In this landscape the 'optimal' and 'near-optimal' (N, C_s) combinations that yield low(est) error-levels at given

computational effort may be identified. Subsequently, a set of eight different 'elemental' error definitions is introduced in Section 3.2. These elemental definitions will be combined to give rise to 'multi-objective' parameter regions. The elemental error definitions cover both large-scale and small-scale flow properties, either evaluated as a strict mathematical L_2-norm, or interpreted as direct physical quantity such as energy or enstrophy. The error definitions will be used in the sequel to provide (N, C_s) combinations that yield near-optimal error-levels for a set of flow properties simultaneously [26].

3.1. Elements of error-landscapes

In Ref. [9], LES of homogeneous isotropic decaying turbulence was performed at various resolutions and Smagorinsky coefficients. Based on these simulation results and a corresponding reference DNS, the overall simulation error based on the resolved kinetic energy $E = \langle \bar{u}_i \bar{u}_i/2 \rangle$ was investigated. Here $\langle\cdot\rangle$ denotes a volume averaging. In order to achieve the required overview of the total error-behavior as function of N and C_s, the time-integrated relative deviation between LES and DNS predictions was evaluated as basic error-measure:

$$\delta_E(N, C_s) = \left[\frac{\int_0^T \left(E_{LES}(t) - E_{\overline{DNS}}(t)\right)^2 dt}{\int_0^T E^2_{\overline{DNS}}(t)\, dt} \right]^{1/2}. \tag{19}$$

Here, T denotes the interrogation time window, E_{LES} is the kinetic energy obtained from a large-eddy simulation at given resolution N and model coefficient C_s, while $E_{\overline{DNS}}$ is the reference solution, obtained by filtering the DNS field with a sharp cut-off filter with filter width $\Delta = h = 1/N$. For consistency we use the *filtered* DNS solution as point of reference [7,39]. In case only unfiltered data are available (e.g. originating from experiments), one should either verify that the filtering has no appreciable effect on the considered reference property, or use an explicit subgrid-scale closure to account for this difference (see e.g. Ref. [40]). We will not address this issue in the present study, but use filtered DNS data in all error definitions.

A range of flow properties can be adopted to characterize different aspects of the evolution of decaying homogeneous turbulence. Analogous to (19), one can define an error based on the resolved enstrophy $\mathcal{E} = \langle \bar{\omega}_i \bar{\omega}_i/2 \rangle$. Here, $\bar{\boldsymbol{\omega}} = \nabla \times \bar{\mathbf{u}}$ is the filtered vorticity. Based on $\mathcal{E}$ one may investigate errors that occur in smaller length-scales of the flow, compared to errors measured in terms of the kinetic energy E. We will also investigate simulation errors in terms of the integral length-scale $\mathcal{L}$, defined as

$$\mathcal{L}(t) = \int_0^\infty f(r,t) dr, \quad f(r,t) = \langle \bar{u}_1(\mathbf{x} + r\mathbf{e}_1, t) \bar{u}_1(\mathbf{x}, t) \rangle / \langle \bar{u}_1^2 \rangle, \tag{20}$$

with $f(r,t)$ the two-point correlation function, $\mathbf{e}_1$ the unit vector in the x_1 direction and $\langle\cdot\rangle$ denoting volume averaging. This may be used to quantify errors in the larger scales.

In Fig. 1a, the error $\delta_E(N, C_s)$ is presented. The errors in the resolved turbulent kinetic energy strongly depend on the resolution and model coefficient. Based on this figure, an 'optimal refinement strategy' can be identified as the 'valley' in this landscape. Such a strategy specifies the coefficients $\widehat{C}_s(N)$ for which the error $\delta_E(N, \widehat{C}_s(N))$ is minimal.

The error-landscape related to $\delta_\mathcal{E}(N, C_s)$ (Fig. 1b) displays error-levels that are considerably higher than those observed for δ_E. The resolved enstrophy is determined to a larger extent by small-scale structures in the flow and hence, more difficult to correctly predict than the resolved kinetic energy. The 'optimal refinement strategy' associated with $\delta_\mathcal{E}$ (cf. Fig. 1b) differs from that seen in Fig. 1a. This dependence of the optimal refinement on the error-definition poses a new challenge to LES error-assessment and optimization, since preferences in error definition are not always objective.

In order to accommodate multiple error-measures into the analysis we first introduce a 'near-optimal' region $\Omega_\delta(a)$ with respect to the error-measure δ as [26]

$$\Omega_\delta(a) = \left\{ (N, C_s) \in \mathbb{R}^2 \left| \frac{\delta(N, C_s)}{\delta(N, \widehat{C}_s(N))} \leqslant 1 + a \right. \right\}. \tag{21}$$

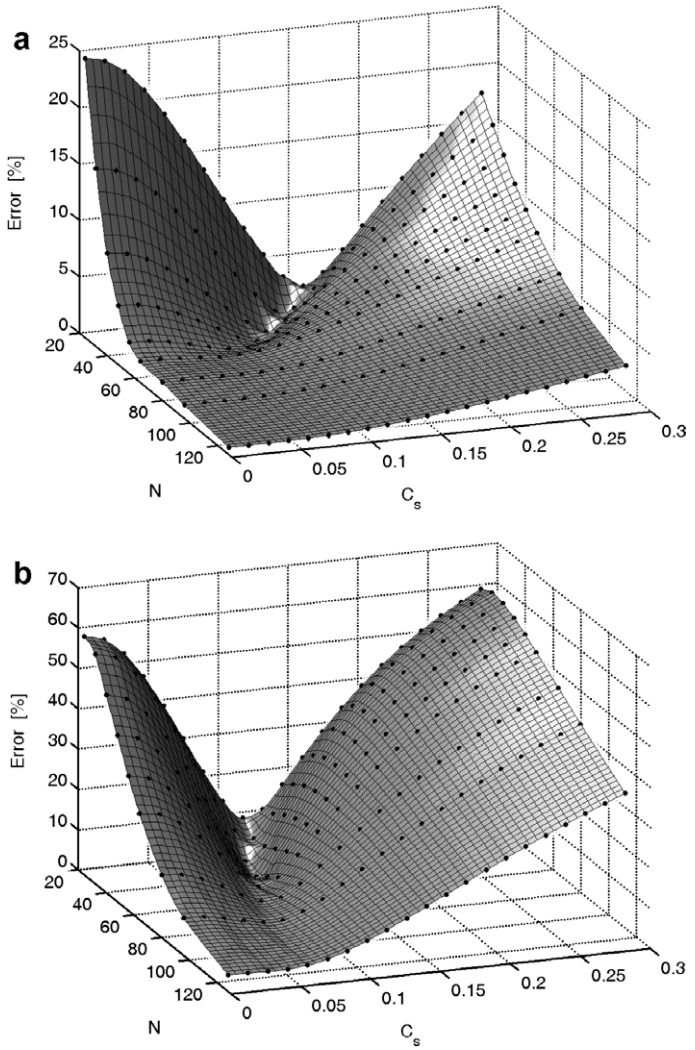

Fig. 1. Error-landscapes of LES employing the Smagorinsky model and the 2–2 discretization. Errors are shown for δ_E (a) and δ_ε (b). The different simulations that were conducted are indicated by (●).

Hence, the 'near-optimal' region contains all values of C_s for which the resulting simulation error δ (i.e., $\delta_\mathcal{L}$, δ_E or δ_ε) is smaller than the minimal error at that resolution N, multiplied by a factor $1 + a$ for $a > 0$. This parameter region corresponds to the 'valley' near the lowest lying optimal refinement strategy in an error-landscape as shown in Fig. 1. Though the selection of the parameter a is somewhat arbitrary, a value $a = 0.2$ is suitable to characterize the main features of these 'error-valleys' and their connectivity [26]. We will use this value for the present study. The shape of the near-optimal region $\Omega_\delta(a)$ provides an overview of the sensitivity of the model, with respect to its optimal error-level.

In Fig. 2, an overview is presented of the error-behavior of the 2–2 discretization in terms of the optimal refinement strategies and 'near-optimal regions' for the three error definitions $\delta_\mathcal{L}$, δ_E and δ_ε. In this figure, the respective optimal Smagorinsky constants are marked with symbols at the different simulation resolutions considered. Moreover, the corresponding 'near-optimal' regions are displayed shaded in gray and semitransparent. As a result, areas in which different near-optimal regions overlap appear in darker shades of gray. Consequently, regions where one, two or three of the considered error-measures are 'near-optimal' can be readily distinguished. As can be observed in Fig. 2, for $N \gtrsim 50$, a connected region exists where all three errors are 'near-optimal'. We will refer to this as a 'multi-objective optimal' region. Note, that the overall

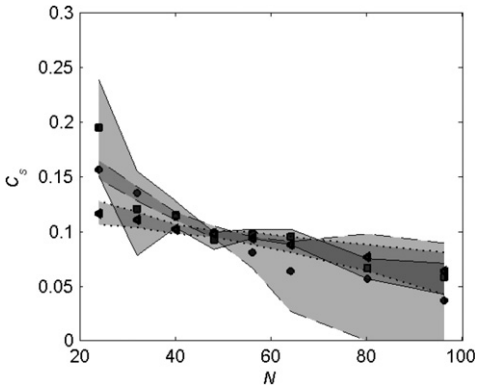

Fig. 2. 'Near optimal' regions of Smagorinsky LES using the 2–2 discretization and error definitions $\delta_{\mathcal{L}}$, δ_{E} and $\delta_{\mathcal{E}}$. Different 'near optimal' regions are shaded gray and semitransparent, such that areas with overlapping near optimal regions appear with darker shades of gray. The curves (—), (––) and (···), respectively, mark the boundaries of the $\delta_{\mathcal{L}}$, δ_{E} and $\delta_{\mathcal{E}}$ 'near optimal' regions. Symbols (■, ●, ◀) correspond respectively to the optimal refinement strategies for these error definitions.

error-level generally decreases with increasing resolution. Hence, the values of $\delta_{\mathcal{L}}$, δ_{E} and $\delta_{\mathcal{E}}$ can vary considerably within the 'near-optimal region', basically decreasing as N increases.

In this computational LES model we observe that for $N \lesssim 50$ no 'multi-objective optimal' region exists that incorporates all three error-measures simultaneously. Though simulations can be optimized with respect to one flow property, by appropriately balancing the interacting modelling and discretization errors, that particular error-balancing can be at the cost of the quality of other predictions. Consequently, LES error evaluation based on a single flow property, may provide a misleading error-assessment, as the 'optimal parameter setting' that is obtained may not yield acceptable accuracy for other flow properties. We will show that this is connected to the selected error-measures and depends also strongly on the numerical discretization schemes.

We next provide an interpretation of the error-measures as weighted integrals of the kinetic energy spectrum. This will also allow to generalize the error definitions $\delta_{\mathcal{L}}$, δ_{E} and $\delta_{\mathcal{E}}$ and will give an indication of the robustness of the error-assessment in the sequel.

3.2. Weighted-spectrum error-measures

For homogeneous isotropic turbulence, one can readily establish that [41]

$$\mathcal{L} = \int_0^\infty k^{-1} E_{\overline{\mathrm{DNS}}}(k,t)\mathrm{d}k, \tag{22}$$

$$E = \int_0^\infty E_{\overline{\mathrm{DNS}}}(k,t)\mathrm{d}k, \tag{23}$$

$$\mathcal{E} = \int_0^\infty k^2 E_{\overline{\mathrm{DNS}}}(k,t)\mathrm{d}k, \tag{24}$$

where $E_{\overline{\mathrm{DNS}}}(k,t)$ denotes the kinetic energy spectrum of the filtered DNS solution, at wavenumber k. Hence, these flow properties are directly related to integrals over the spectrum, weighted with an appropriate power of k. Using these expressions, the errors $\delta_{\mathcal{L}}$, δ_{E} and $\delta_{\mathcal{E}}$ can be written in terms of weighted-spectrum integrals as well. Taking for $\overline{(\cdot)}$ a sharp cut-off filter with cut-off wavenumber k_{c}, we introduce

$$D_p(N, C_{\mathrm{s}}) = \left[\frac{\int_0^T \left\{ \int_0^{k_{\mathrm{c}}} k^p (E_{\mathrm{LES}}(k,t) - E_{\mathrm{DNS}}(k,t))\mathrm{d}k \right\}^2 \mathrm{d}t}{\int_0^T \left\{ \int_0^{k_{\mathrm{c}}} k^p E_{\mathrm{DNS}}(k,t)\mathrm{d}k \right\}^2 \mathrm{d}t} \right]^{1/2}. \tag{25}$$

In this definition, the cut-off filter is visible in the upper limit k_{c} of the inner integral. The error-measures based on (22)–(24) can readily be identified as $\delta_{\mathcal{L}} = D_{-1}$, $\delta_{\mathrm{E}} = D_0$ and $\delta_{\mathcal{E}} = D_2$. Errors in large-scale properties are

characterized best by low values of p while small-scale errors are associated with higher values of p. Apart from $p = -1$, 0 and 2, we will also include $p = 1$ in the sequel. Though the error D_1 does not directly correspond to a well-known flow property, it is included since it completes the sequence of error-measures for $p = -1$, 0, 1, 2.

One may observe that expression (25) does not present a true norm of the weighted energy spectra. Consequently, these error measures may yield relatively small values, not because errors are actually small but because errors in the LES spectrum at different wavenumbers may partially cancel each other. Error-contributions from k-regions in which the DNS-spectrum is under-predicted may be compensated by an over-predicted spectrum at other wavenumbers. This can lead to underestimation of the actual error. Therefore, we will also incorporate the following error-definition [26]:

$$d_p(N, C_s) = \left[\frac{\int_0^T \int_0^{k_c} k^{2p} (E_{\mathrm{LES}}(k,t) - E_{\mathrm{DNS}}(k,t))^2 \mathrm{d}k\, \mathrm{d}t}{\int_0^T \int_0^{k_c} k^{2p} (E_{\mathrm{DNS}}(k,t))^2 \mathrm{d}k\, \mathrm{d}t} \right]^{1/2}. \tag{26}$$

This error definition is such that every deviation of the LES spectrum from the DNS-spectrum is added as a positive contribution to the total error. The errors d_p cannot be interpreted in terms of well-known physical flow properties. Still, these error-measures can likewise be adopted to quantify the total simulation error in large-scale as well as small-scale flow properties.

In the next section, we will use both error definitions D_p and d_p to quantify the error-behavior associated with the different finite-volume discretizations introduced in Section 2. For these schemes we will determine the multi-objective optimal refinement strategies. We will also compare the error-levels along such a 'multi-objective optimal' refinement strategy.

4. Evaluation of different numerical-schemes

In this section, we compare the induced error-behavior of the different finite-volume discretizations using the error-landscape methodology presented in the previous section. We will incorporate both error definitions D_p and d_p to compare an error-measure in terms of well-known physical flow properties to an error-measure based on a mathematical norm. For sake of comparison, we will focus in particular on a weighted optimal refinement strategy that includes errors at different p. The error-levels along these trajectories show a considerable dependency on the spatial discretization method that was adopted. The dependence of the trajectories themselves on the precise error definition, i.e., D_p or d_p, is shown to be quite small.

Near-optimal regions based on D_p ($p = -1$ to 2) are presented in Fig. 3a–d for all discretization schemes considered. The optimal refinement strategies $\widehat{C}_s^{(p)}(N)$ for different p are indicated by symbols. Large differences appear between the four finite-volume discretizations. The absence of connected 'multi-objective optimal' regions for some resolution ranges in Fig. 3a–d again emphasizes that LES evaluations using a limited number of physics-based error-measures, may lead to inaccurate perceptions of simulation quality. We notice that the 2–2 method has the most extended 'multi-objective optimal' region starting at resolutions $N \approx 40$. The 4–4 method has a somewhat smaller multi-objective optimal region, i.e., a connected parameter region in which all error-measures are within the pre-specified acceptance range, is found only for resolutions $N \geqslant 56$. The 4–2 method has almost no multi-objective optimal region in the considered resolution range; full overlap only occurs for $N \geqslant 80$. Finally, the 2–4 method displays a multi-objective optimal region for $N \geqslant 64$. This region is situated around $C_s = 0$, indicating that LES using this numerical method (and $N \geqslant 64$) performs best without the use of the Smagorinsky model.

In Fig. 4a–d, multi-objective optimal regions are presented for the different finite-volume schemes, but now based on the errors d_p ($p = -1$ to 2). In contrast to Fig. 3, connected multi-objective optimal regions exist for all numerical-schemes over the entire resolution range considered. The extent of the multi-objective parameter regions is considerably larger than seen in Fig. 3 and quite comparable among the different finite-volume discretizations. However, one can also observe differences in the location of these multi-objective regions for the different schemes. The 4–2 multi-objective region requires the highest coefficients C_s to comply with the imposed accuracy conditions. The parameter region for the 2–4 scheme has the lowest C_s values. Both 2–2 and 4–4 schemes are situated in between.

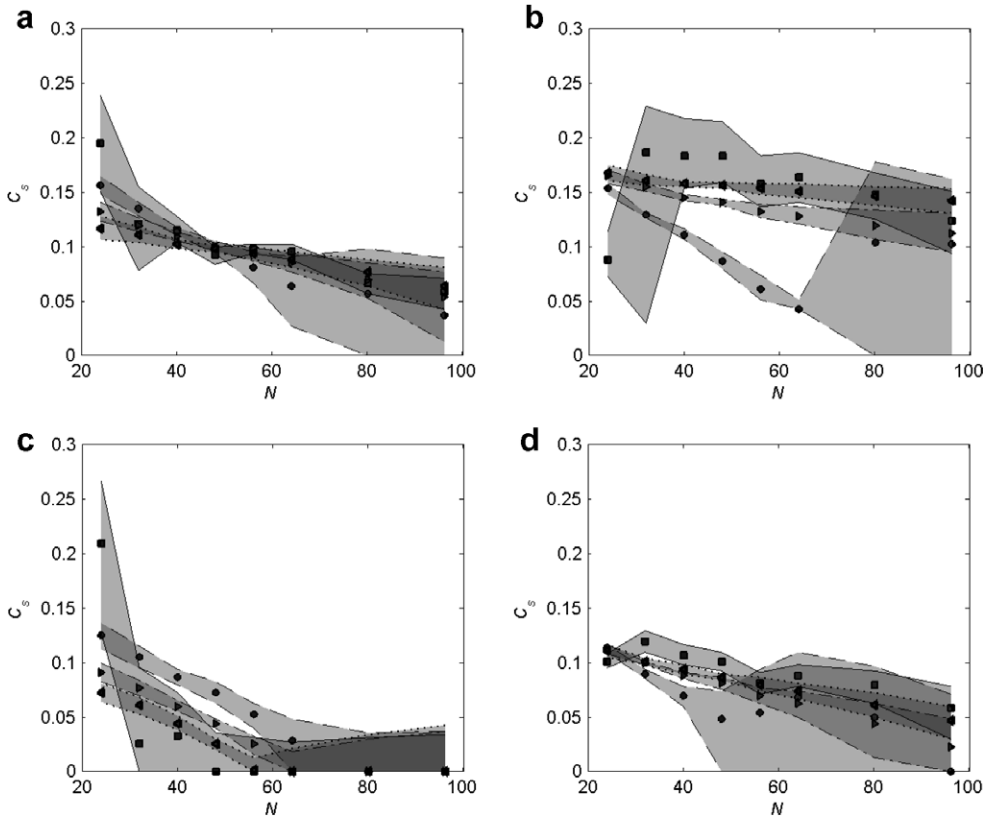

Fig. 3. 'Near optimal' regions based on D_p ($p = -1$ to 2) for the 2–2 scheme (a), the 4–2 scheme (b), the 2–4 scheme (c) and the 4–4 scheme (d). Different 'near optimal' regions are displayed in gray and semitransparent, such that regions with overlap appear with darker shades of gray. The curves (—), (– –), (-·) and (···), respectively, mark the boundaries of the D_{-1} ($=\delta_{\mathcal{L}}$), D_0 ($=\delta_E$), D_1 and D_2 ($=\delta_{\mathcal{E}}$) 'near optimal' regions. Symbols (■, ●, ▶, ◀) correspond, respectively, to the optimal refinement strategies for the different error definitions.

In order to compare 'optimal' refinement strategies of C_s and to evaluate the error-levels along such a selection of C_s, we introduce multi-objective optimal refinement strategies $\widetilde{C}_D(N)$ and $\widetilde{C}_d(N)$ associated with either $\{D_p\}$ or $\{d_p\}$. These refinement strategies $\widetilde{C}_D(N)$ and $\widetilde{C}_d(N)$ are the respective optimal strategies associated with the weighted errors [26]

$$\widetilde{D}(N, C_s) = \frac{\sum_p [D_p(N, C_s)/D_p(N, \widehat{C}_s^{(p)}(N))]}{\sum_p [1/D_p(N, \widehat{C}_s^{(p)}(N))]}, \tag{27}$$

$$\tilde{d}(N, C_s) = \frac{\sum_p [d_p(N, C_s)/d_p(N, \widehat{C}_s^{(p)}(N))]}{\sum_p [1/d_p(N, \widehat{C}_s^{(p)}(N))]}. \tag{28}$$

In the definition of $\tilde{d}$ (and $\widetilde{D}$), the different errors $d_p(N, C_s)$ are compensated with their respective optimal error-levels $d_p(N, \widehat{C}_s^{(p)}(N))$, evaluated at the optimal refinement strategies $\widehat{C}_s^{(p)}$ that were introduced in connection to Fig. 3a–d above. This ensures that error-measures with quite different levels can be combined properly. For example, errors d_2 which are considerably higher than d_{-1}, do not dominate the weighted error $\tilde{d}$ because of this p-dependent scaling. The definitions of $\widetilde{C}_d(N)$ and $\widetilde{C}_D(N)$ are such that these curves are situated inside the multi-objective optimal regions seen in Figs. 3 and 4 where these exist.

A comparison between the multi-objective optimal refinement strategies $\widetilde{C}_d$ and $\widetilde{C}_D$ is presented in Fig. 5 for all four finite-volume discretizations. Differences between $\widetilde{C}_d$ and $\widetilde{C}_D$ due to differences between $\tilde{d}$ and $\widetilde{D}$ are relatively small compared to the influence arising from the selected discretization scheme. Hence, despite the rather different interpretations associated with the error-measures D_p and d_p, the suggested optimal refinement

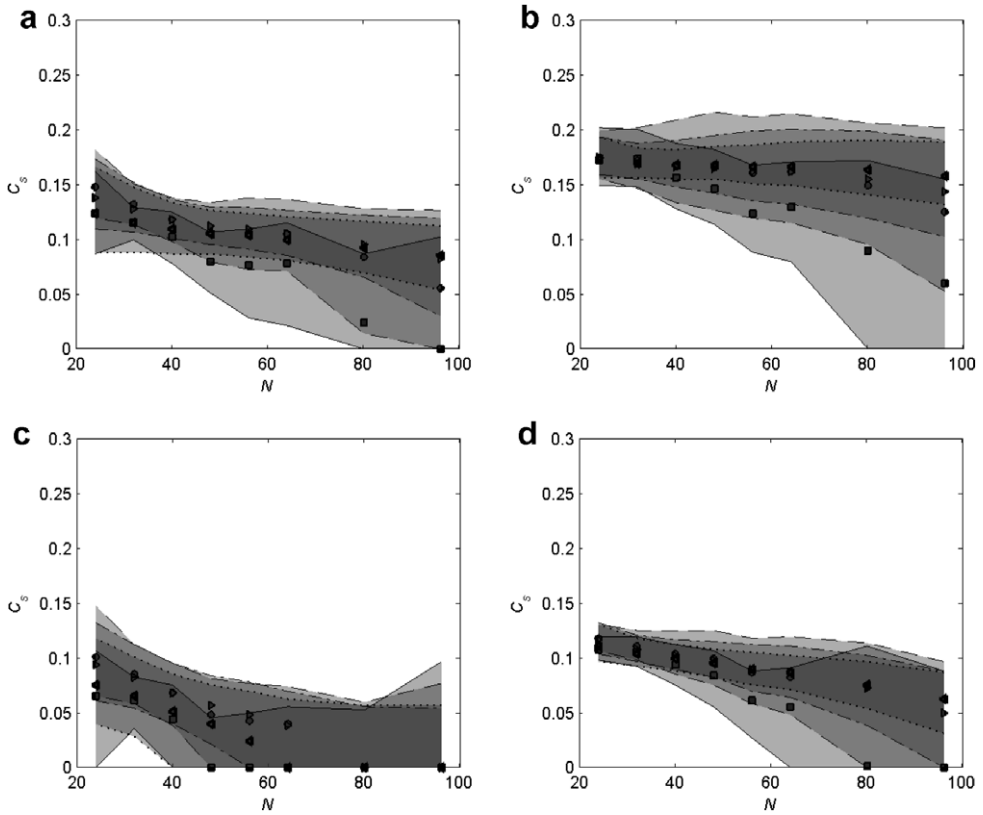

Fig. 4. 'Near optimal' regions based on d_p ($p = -1$ to 2) for the 2–2 scheme (a), the 4–2 scheme (b), the 2–4 scheme (c) and the 4–4 scheme (d). Different 'near optimal' regions are displayed in gray and semitransparent, such that regions with overlap appear with darker shades of gray. The curves (—), (– –), (–·) and (···), respectively, mark the limits of the d_{-1}, d_0, d_1 and d_2 'near optimal' regions. Symbols (■, ●, ▶, ◀) correspond, respectively, to the optimal refinement strategies for the different error definitions.

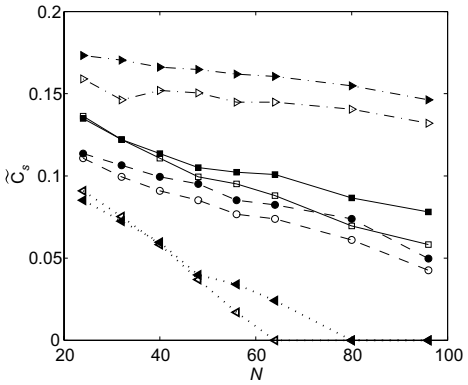

Fig. 5. Multi-objective refinement strategies $\widetilde{C}_s$ (cf. (27), (28)) as function of the resolution N for the 2–2 scheme $\left(-\boxplus\right)$, the 4–2 scheme $\left(-\triangleright\right)$, the 2–4 scheme $\left(\cdot\,\triangleleft\right)$ and the 4–4 scheme $\left(-\circ-\right)$. Opens symbols: using $\{D_p\}$; Closed symbols: using $\{d_p\}$.

strategies arising from the weighted error-measures are predicted in a robust manner. The optimal refinement strategies occur in well-distinguished pairs that are characteristic for the finite-volume method that was adopted. For instance, comparatively large values of C_s are required to diminish numerical effects of under-resolution in the 4–2 scheme. The comparable behavior of the 2–2 and 4–4 schemes in Figs. 3 and 4 is now

displayed by quite comparable levels of $\widetilde{C}$ to achieve optimal error-reduction. Finally, the overall C_s-level associated with optimal performance of the 2–4 method is lowest; this computational model appears not to benefit much from adding an explicit Smagorinsky subgrid term to the LES equations.

The relative positions of the different optimal refinement strategies correlate well with results from a modified wavenumber analysis [42,15]. In fact, from such an analysis it becomes clear that the convective transfer of kinetic energy toward the smaller scales is less under-predicted by the fourth-order discretization, compared to the second-order method. Likewise, the dissipative fluxes are under-predicted more by the second-order method compared to the fourth-order viscous discretization. Thus, it appears natural that the optimal refinement strategy of the 4–2 method requires largest values of the Smagorinsky constant. Among the methods considered, the strongest convective energy transfer is coupled to the weakest representation of the dissipation—this requires largest additional damping by the subgrid model in order to reach optimal accuracy. In the same vein the relative position of the 2–4 method's optimal line may be interpreted. This correlation may be helpful in other situations as well, although one should realize that this argument based on modified wavenumbers cannot include dynamic accumulation of discretization error effects [14].

We next turn to a comparison between the level of errors along the refinement strategies $\widetilde{C}_d$ and $\widetilde{C}_D$. An overview of the results is presented in Fig. 6. We observe that errors related to d_p are considerably higher than those based on D_p, again illustrating the effect of partial error-cancellations in the latter. Generally, the 2–2 and 4–4 schemes give rise to the lowest optimal errors, followed by the 'mixed-order' schemes. The 2–4 scheme appears quite accurate as well, primarily for the larger-scale flow properties. The 4–2 scheme yields highest error-levels for most resolutions. Striking qualitative differences may be observed between the 'convergence patterns' associated with D_p and d_p. A reasonably monotonous decrease of the error-levels occurs as function of the resolution N when use is made of $\{d_p\}$. However, strong fluctuations in the optimal error-levels may occur as function of N when use is made of $\{D_p\}$. In terms of this error-measure, an increase in resolution not necessarily leads to an increased accuracy of predictions. However, also when $\{D_p\}$ is adopted, the use of 'equal-order' finite-volume methods (2–2 and 4–4) appears to be advisable over the 'mixed-order' methods. This is a central finding in this paper. It appears sub-optimal to increase the accuracy with which the convective fluxes are evaluated if not also the viscous terms are treated more accurately as well.

An extension of Lilly's analysis [43] was recently proposed in [44] which allows a theoretical estimation of the Smagorinsky coefficient as function of the Reynolds number and the resolution, that is consistent with subgrid dissipation requirements. This analysis is based on an idealized analytical representation of the energy spectrum. The dissipation added by the Smagorinsky model was required to coincide with the theoretical subgrid dissipation corresponding to the assumed spectrum and filter width. This yields a Smagorinsky coefficient $C_s^*(\Delta, Re)$, which depends on the filter width Δ and the Reynolds number, i.e.

$$C_s^*(\Delta, Re) = \frac{C_{s,\infty}}{\gamma} \Phi^{-3/4} \sqrt{1 - \left(\frac{\gamma\eta}{C_{s,\infty}\Delta}\right)^{4/3}}\, \Phi. \tag{29}$$

In this formula, the function $\Phi(\Delta, Re)$ is of order unity and depends on the energy spectrum, $C_{s,\infty}$ is Lilly's Smagorinsky constant, γ is a filter-shape correction and η the Kolmogorov scale. More details can be found in Ref. [44]. In Fig. 7, we compare the predicted $C_s^*(N)$ by this formula (using $N = 1/\Delta$) to $\widetilde{C}_D$ and $\widetilde{C}_d$.

The theoretical trajectory $C_s^*(N)$ coincides very well with the 'multi-objective optimal strategies' for the 2–2 scheme. If we accept this correlation to also hold approximately at other flow conditions, then the theoretically predicted C_s^* could provide a near-optimal refinement strategy for much higher Reynolds numbers as well. We observe in Fig. 7 that an increase in Re implies a higher value for C_s^* in order to obtain optimal accuracy at given resolution. As $Re \to \infty$ the dependence on resolution N appears to diminish and an optimal value of $C_s = 0.142$ [44] is found. Future research will be directed to test this correspondence between C_s^* and $\widetilde{C}_D$, $\widetilde{C}_d$ at other flow conditions as well.

As a final assessment of the differences in error-behavior between the four discretization methods, we consider the three-dimensional energy spectra at Smagorinsky constants chosen along the d_p-multi-objective optimal strategies for resolutions $N = 24, 32, \ldots, 96$. Results are shown in Fig. 8a–d for spectra at $t = 0.8$, i.e., toward the end of the simulation in which case the effects due to the numerical method have had considerable time to develop. The prediction of the spectra was not 'optimized' directly as it was not explicitly included in

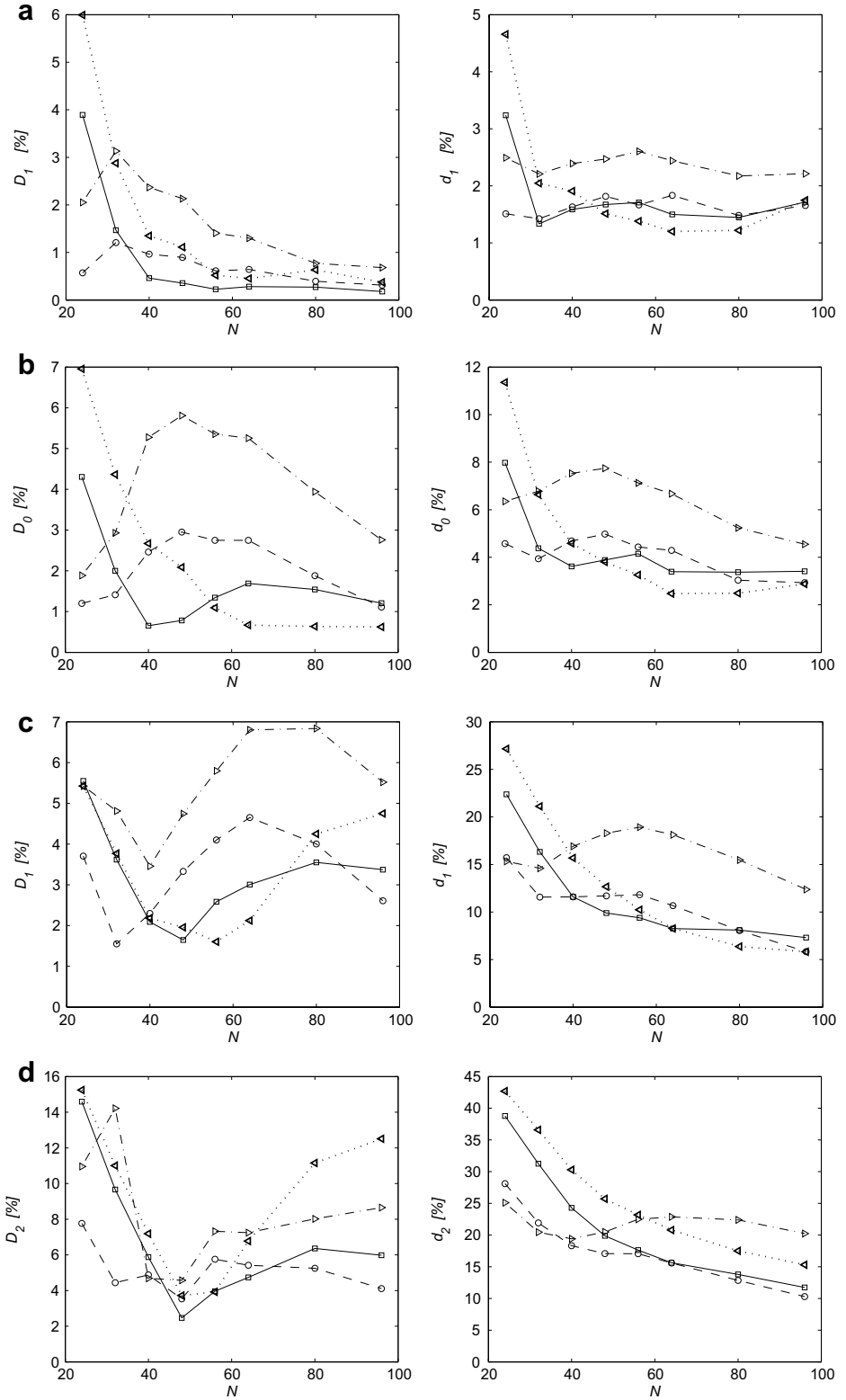

Fig. 6. Comparisons of relative errors D_p (left) and d_p (right) for $p = -1$ (a), $p = 0$ (b), $p = 1$ (c) and $p = 2$ (d), along the multi-objective optimal refinement strategy $\widetilde{C}_D$ (*left*) and $\widetilde{C}_d$ (right) for the 2–2 scheme $\left(-\boxplus\right)$, the 4–2 scheme $\left(-\triangleright\right)$, the 2–4 scheme $\left(\cdot\,\triangleleft\right)$ and the 4–4 scheme $\left(-\circ-\right)$.

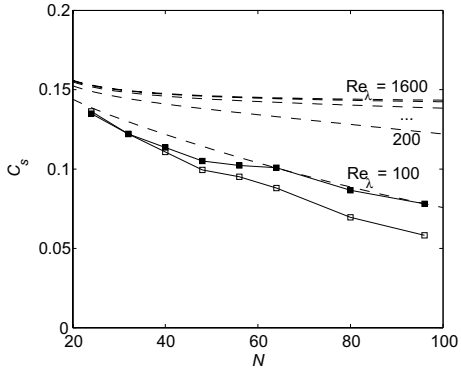

Fig. 7. Theoretical $C_s^*(N)$ lines (––) at different Reynolds numbers ($Re_\lambda = 100, 200, 400, 800, 1600$) and multi-objective refinement strategies $\widetilde{C}_s$ for the 2–2 scheme (⊣⊟). Opens symbols: using $\{D_p\}$ and closed symbols: using $\{d_p\}$.

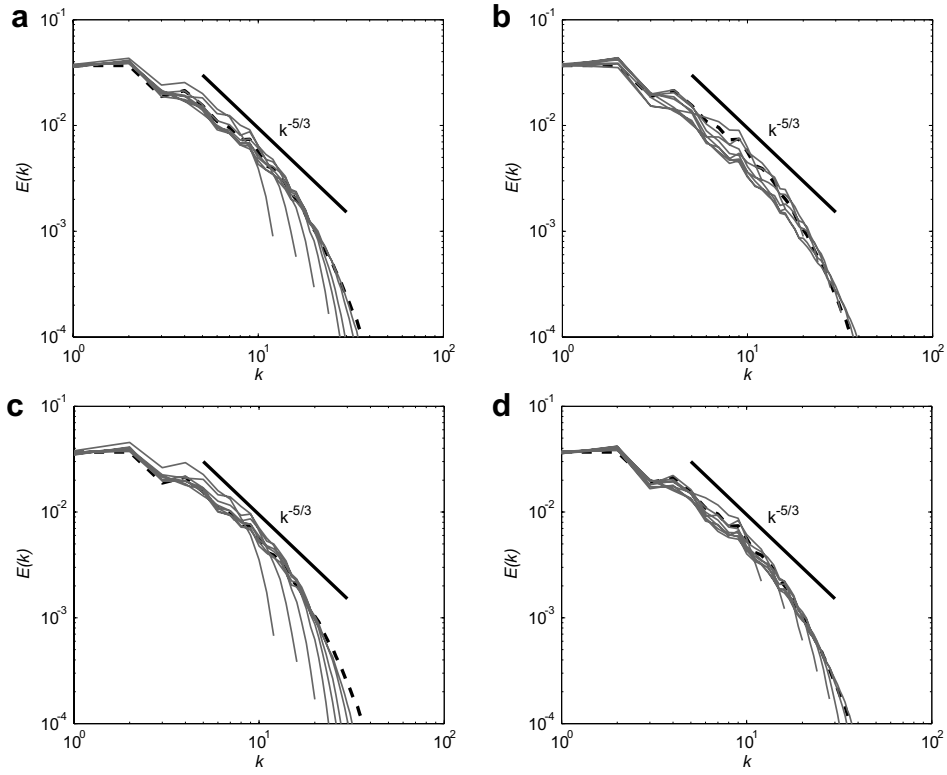

Fig. 8. LES spectra (gray lines) at $t = 0.8$ along the respective $\{d_p\}$-multi-objective refinement trajectories ($N = 24, 32, 40, 48, 56, 64, 80, 96$) for the 2–2 scheme (a), the 4–2 scheme (b), the 2–4 scheme (c) and the 4–4 scheme (d). (––): DNS reference solution.

the error-measures, but only through its 'moments'. We notice that all spectra do capture the general shape seen in the DNS result, including a segment with approximately $-5/3$ scaling. The 2–2 and 4–4 discretization methods and to a slightly lesser degree the 4–2 scheme, display quite low levels of error, while the 2–4 scheme presents a less clear convergence to the DNS spectrum, with increasing resolution.

In this figure, we notice characteristic differences between a second- and a fourth-order discretization of the convective terms (i.e., Fig. 8a, c (left) versus b, d (right)). The fourth-order (convective) schemes (4–4 and 4–2) clearly predict more energy in the tail of the spectra than the second-order schemes (2–2 and 2–4). In terms of

the modified wavenumber associated with second and fourth-order methods [42,15], this can be attributed to a relatively higher energy transfer to the small-scales for the fourth-order schemes. In the second-order methods, the discretization error partially inhibits the energy-cascade process. This corresponds well with findings reported in [14].

5. Conclusions

An assessment of LES errors has been made for a variety of central finite-volume discretizations. This was based on the evaluation of multiple flow properties simultaneously [26]. The Smagorinsky eddy-viscosity model was adopted in simulations of homogeneous decaying turbulence. It was shown that values for the Smagorinsky coefficient exist as function of the simulation resolution N such that all considered flow quantities are predicted nearly optimally if N is sufficiently large. A strong dependence of the near-optimal Smagorinsky coefficients on the adopted finite-volume scheme was established.

Both mathematics-based L_2-norms ($\{d_p\}$) and physics-based ($\{D_p\}$) error definitions were considered. It was shown that physics-based errors may lead to inaccurate perceptions on LES quality when only a single flow property is considered. However, in many practical applications, only physics-based flow properties are available. A pragmatic solution to this dilemma was proposed. We demonstrated that, if a range of small- and large-scale errors is included simultaneously in the analysis, robust conclusions can be formulated regarding the error-behavior of a particular finite-volume discretization. The multi-objective optimal refinement strategies $\widetilde{C}_d(N)$ and $\widetilde{C}_D(N)$ appear in closely matched pairs. The location of these refinement strategies is strongly dependent on the discretization method. The relative locations of these strategies may be interpreted in terms of modified wavenumbers associated with the second or fourth-order discretizations of the convective and viscous fluxes.

The error dynamics of Smagorinsky LES has been investigated at $\Delta = h$ for different numerical implementations. Second- and fourth-order central finite-volume discretizations were considered for the convective and viscous terms, leading to four possible combinations (i.e., the 2–2, 2–4, 4–2 and 4–4 schemes). A comparison of multi-objective optimal refinement strategies $\widetilde{C}_s(N)$ indicates that the 4–2 scheme requires the highest Smagorinsky constants in order to yield acceptable simulation results. The $\widetilde{C}_s(N)$ levels for the 2–2 and 4–4 schemes are considerably lower. Further, the 2–4 scheme has the lowest $\widetilde{C}_s(N)$: for $N > 64$ this discretization scheme yields best results even without the use of a Smagorinsky model.

We observed that the 2–2 generally displayed the smallest errors at coarser subgrid resolutions, closely followed by the 4–4 scheme. The 'mixed-order' combinations yield higher total errors. This illustrates that, at coarse resolutions, the asymptotic error behavior as expressed by the order of the spatial discretization is not a suitable indicator for the total error in large-eddy simulations. The use of 'equal-order' finite-volume methods (2–2 and 4–4) appears to be advisable over the 'mixed-order' methods.

We evaluated a theoretical relation $C_s^*(N)$ [44] which expresses the Smagorinsky coefficient as function of the filter width and the Reynolds number. The 2–2 multi-objective refinement trajectory $\widetilde{C}_s(N)$ was found to be well approximated by C_s^*. This correspondence requires further research in different test cases. Based on this theoretical relation we predicted for infinite Reynolds numbers a constant multi-objective refinement strategy for the 2–2 scheme, situated at $C_s \approx 0.142$.

In the current work, we presented a methodology for the evaluation of errors in large-eddy simulations. Its strengths were demonstrated by comparing in detail the quality of various finite-volume discretization methods for LES employing a Smagorinsky model. Obviously, some of the conclusions in the current work are specific to the employed subgrid-scale closure and the class of discretization methods. Nevertheless, the observed trends clearly illustrate the intricate error behavior which may be encountered in LES and the need for a strict framework for error evaluation and comparison of LES methods. We believe that such a framework will be a valid tool for evaluations of subgrid-scale models and discretization schemes.

We focussed on simulations of homogeneous isotropic turbulence. Flows of more realistic complexities, including, e.g. channel flows, mixing layers and jets, require a more involved analysis. A foretaste on the intricate error-behavior which can arise, may be obtained from Ref. [45], discussing the error evaluation of unresolved channel flow DNS. Extensions towards modelled LES, both for a mixing layer and for channel flows are topics of ongoing research.

References

[1] P. Sagaut, Large eddy simulations for incompressible flows, Scientific Computation, third ed., Springer-Verlag, 2006.
[2] B.J. Geurts, Elements of Direct and Large-Edddy Simulation, R.T. Edwards Inc., Flourtown, 2003.
[3] R.S. Rogallo, R. Moin, Numerical simulations of turbulent flows, Annual Review in Fluid Mechanics 16 (1984) 99–137.
[4] U. Frisch, Turbulence, Cambridge University Press, 1995.
[5] C. Meneveau, Statistics of turbulence subgrid-scale stresses: necessary conditions and experimental tests, Physics of Fluids 6 (2) (1994) 815–833.
[6] S. Ghosal, An analysis of numerical errors in large-eddy simulations of turbulence, Journal of Computational Physics 125 (1996) 187–206.
[7] B. Vreman, B. Geurts, H. Kuerten, Comparison of numerical schemes in large-eddy simulations of the temporal mixing layer, International Journal for Numerical Methods in Fluids 22 (1996) 297–311.
[8] B.J. Geurts, J. Fröhlich, A framework for predicting accuracy limitations in large eddy simulations, Physics of Fluids 14 (6) (2002) L41–L44.
[9] J. Meyers, B.J. Geurts, M. Baelmans, Database-analysis of errors in large-eddy simulation, Physics of Fluids 15 (9) (2003) 2740–2755.
[10] P. Sagaut, M. Ciardi, A finite-volume variational multiscale method coupled with a discrete interpolation filter for LES of isotropic turbulence and fully developed channel flow, Physics of Fluids 18 (11) (2006) 115101.
[11] V. Levasseur, P. Sagaut, M. Mallet, Subgrid models for large-eddy simulation using unstructured grids in a stabilized finite element framework, Journal of Turbulence 7 (2006) N28.
[12] F.K. Chow, P. Moin, A further study of numerical errors in large-eddy simulations, Journal of Computational Physics 184 (2003) 366–380.
[13] I. Fedioun, N. Lardjane, I. Gökalp, Revisiting numerical errors in direct and large eddy simulations of turbulence: physical and spectral analysis, Journal of Computational Physics 174 (2001) 816–851.
[14] N. Park, K. Mahesh, Analysis of numerical errors in large eddy simulation using statistical closure theory, Journal of Computational Physics 222 (2007) 194–216.
[15] B.J. Geurts, F. van der Bos, Numerically induced high-pass dynamics in large-eddy simulation, Physics of Fluids 17 (12) (2005) 125103.
[16] S. Stolz, N.A. Adams, An approximate deconvolution procedure for large-eddy simulation, Physics of Fluids 11 (7) (1999) 1699–1701.
[17] S. Hickel, N.A. Adams, J.A. Domaradzki, An adaptive local deconvolution method for implicit LES, Journal of Computational Physics 231 (2006) 413–436.
[18] G. De Stefano, O.V. Vasilyev, "Perfect" modeling framework for dynamic SGS model testing in large eddy simulation, Theoretical and Computational Fluid Dynamics 18 (2004) 27–41.
[19] B.J. Geurts, Inverse modeling for large-eddy simulation, Physics of Fluids 9 (12) (1997) 3585–3587.
[20] J. Meyers, M. Baelmans, C. Lacor, A generalised view on mixed models, in: C. Dopazo (Ed.), Advances in Turbulence VIII, Proceedings of the Eight European Turbulence Conference, 2000, pp. 515–518.
[21] D. Carati, G.S. Winckelmans, H. Jeanmart, On the modelling of the subgrid-scale and filtered-scale stress tensors in large-eddy simulation, Journal of Fluid Mechanics 441 (2001) 119–138.
[22] J.C. Magnient, P. Sagaut, M. Deville, A study of build-in filter for some eddy-viscosity models in large-eddy simulation, Physics of Fluids 13 (5) (2001) 1440–1449.
[23] C. Foias, D.D. Holm, E.S. Titi, The Navier–Stokes-alpha model of fluid turbulence, Physica D-Nonlinear Phenomena 152 (2001) 505–519.
[24] B.J. Geurts, D.D. Holm, Regularization modeling for large-eddy simulation, Physics of Fluids 15 (1) (2003) L13–L16.
[25] J. Meyers, B.J. Geurts, M. Baelmans, Optimality of the dynamic procedure for large-eddy simulations, Physics of Fluids 17 (4) (2005) 045108.
[26] J. Meyers, P. Sagaut, B.J. Geurts, Optimal model parameters for multi-objective large-eddy simulations, Physics of Fluids 18 (2006) 095103.
[27] M. Germano, U. Piomelli, P. Moin, W.H. Cabot, A dynamic subgrid-scale eddy viscosity model, Physics of Fluids A 3 (7) (1991) 1760–1765.
[28] B.J. Geurts, J. Meyers, Successive inverse polynomial interpolation to optimize Smagorinsky's model for large-eddy simulation of homogeneous turbulence, Physics of Fluids 18 (11) (2006) 118102.
[29] Y. Morinishi, T.S. Lund, O.V. Vasilyev, P. Moin, Fully conservative higher order finite difference schemes for incompressible flow, Journal of Computational Physics 143 (1998) 90–124.
[30] O.V. Vasilyev, High order finite difference schemes on non-uniform meshes with good conservation properties, Journal of Computational Physics 157 (2000) 746–761.
[31] R.W.C.P. Verstappen, A.E.P. Veldman, Symmetry-preserving discretization of turbulent flow, Journal of Computational Physics 187 (2003) 343–368.
[32] J. Smagorinsky, General circulation experiments with the primitive equations: I. The basic experiment, Monthly Weather Review 91 (3) (1963) 99–165.
[33] B. Vreman, B. Geurts, H. Kuerten, A priori tests of large eddy simulation of the compressible plane mixing layer, Journal of Engineering Mathematics 29 (1995) 299–327.
[34] B. Vreman, B. Geurts, H. Kuerten, Large-eddy simulation of the turbulent mixing layer, Journal of Fluid Mechanics 339 (1997) 357–390.

[35] W. Ijzerman, Signal representation and modeling of spatial structures in fluids, Ph.D. thesis, Universiteit Twente, 2000.
[36] A. Jameson, Transonic flow calculations, MAE-Report 1651, Princeton University, 1983.
[37] C. Hirsch, Fundamentals of numerical discretization, Numerical Computation of Internal and External Flows, vol. 1, John Willey & Sons, 1988.
[38] T.H. Lê, B. Troff, P. Sagaut, K. Dang-Tran, T.P. Loc, PEGASE: a Navier–Stokes solver for direct numerical simulation of incompressible flows, International Journal for Numerical Methods in Fluids 24 (1997) 833–861.
[39] G.S. Winckelmans, H. Jeanmart, D. Carati, On the comparison of turbulence intensities from large-eddy simulation with those from experiment or direct numerical simulation, Physics of Fluids 14 (5) (2002) 1809–1811.
[40] J. Meyers, M. Baelmans, Determination of subfilter energy in large-eddy simulations, Journal of Turbulence 5 (026) (2004).
[41] S.B. Pope, Turbulent Flows, Cambridge University Press, 2000.
[42] S.K. Lele, Compact finite difference schemes with spectral-like resolution, Journal of Computational Physics 103 (1992) 16–42.
[43] D.K. Lilly, The representation of small-scale turbulence in numerical simulation experiments, in: Proceedings of IBM Scientific Computing Symposium on Environmental Sciences, IBM Data Processing Division, White Plains, New York, 1967.
[44] J. Meyers, P. Sagaut, On the model coefficients for the standard and the variational multi-scale Smagorinsky model, Journal of Fluid Mechanics 569 (2006) 287–319.
[45] J. Meyers, P. Sagaut, Is plane-channel flow a friendly case for the testing of LES subgrid-scale models? Physics of Fluids 19 (2007) 048105.